









Please cite the Published Version

Hussein, Shaimaa , Mahmoud, Ayman M , Elgebaly, Hassan A , Hendawy, Omnia Magdy , Hassanein, Emad H M , Moustafa, Shaima M N , Alotaibi, Nasser F  and Nassar, Amr M 
(2022) Green Synthesis of Trimetallic Nanocomposite (Ru/Ag/Pd)-Np and Its In Vitro Antimicrobial and Anticancer Activities. Journal of Chemistry, 2022. 4593086 ISSN 2090-9063

DOI: <https://doi.org/10.1155/2022/4593086>

Publisher: Hindawi Limited

Version: Published Version

Downloaded from: <https://e-space.mmu.ac.uk/635741/>

Usage rights:  [Creative Commons: Attribution 4.0](https://creativecommons.org/licenses/by/4.0/)

Additional Information: This is an open access article which first appeared in Journal of Chemistry








Data Access Statement: The data supporting the findings of this study are included within the article and its supplementary materials.

Enquiries:

If you have questions about this document, contact openresearch@mmu.ac.uk. Please include the URL of the record in e-space. If you believe that your, or a third party's rights have been compromised through this document please see our Take Down policy (available from <https://www.mmu.ac.uk/library/using-the-library/policies-and-guidelines>)

Research Article

Green Synthesis of Trimetallic Nanocomposite (Ru/Ag/Pd)-Np and Its In Vitro Antimicrobial and Anticancer Activities

Shaimaa Hussein ¹, Ayman M. Mahmoud ², Hassan A. Elgebaly ³,
Omnia Magdy Hendawy ¹, Emad H. M. Hassanein ⁴, Shaima M. N. Moustafa ⁵,
Nasser F. Alotaibi ⁶ and Amr M. Nassar ⁶

¹Department of Pharmacology, College of Pharmacy, Jouf University, Sakaka 72341, Aljouf, Saudi Arabia

²Physiology Division, Zoology Department, Faculty of Science, Beni-Suef University, Beni-Suef, Egypt

³Department of Biology, College of Science, Jouf University, Sakaka, Saudi Arabia

⁴Department of Pharmacology and Toxicology, Faculty of Pharmacy, Al-Azhar University, Assiut, Egypt

⁵Biology Department College of Science, Jouf University, P.O. Box 2014, Sakaka, Saudi Arabia

⁶Chemistry Department, College of Science, Jouf University, Sakaka, Saudi Arabia

Correspondence should be addressed to Amr M. Nassar; amnassar@ju.edu.sa

Received 2 June 2022; Revised 9 July 2022; Accepted 22 August 2022; Published 15 September 2022

Academic Editor: Ashanul Haque

Copyright © 2022 Shaimaa Hussein et al. This is an open access article distributed under the Creative Commons Attribution License, which permits unrestricted use, distribution, and reproduction in any medium, provided the original work is properly cited.

In this study, we used the aqueous extract of garlic tunicate leaf to reduce a mixture of equal amounts of ruthenium chloride, silver nitrate, and palladium acetate for the biosynthesis of ruthenium/silver/palladium trimetallic nanocomposite (Ru/Ag/Pd)-Np. Some physicochemical tools were used for nanocomposite characterization, including Fourier-transform infrared spectroscopy (FT-IR), X-ray diffraction (XRD), thermal gravimetric analysis (TGA), UV-Vis spectroscopy (UV-Vis), scanning electron microscope (SEM), and transmittance electron microscope (TEM). XRD revealed that the crystal size of the nanocomposite is 15.67 nm. The TEM images showed that the particle size ranged 50–90 nm. The antimicrobial efficacy of the nanocomposite was examined against *Aspergillus flavus*, *Aspergillus niger*, *Candida albicans*, *Candida glabrata*, *Escherichia coli*, and *Bacillus cereus*. The results showed a potent antimicrobial activity toward all tested microorganisms. (Ru/Ag/Pd)-Np showed antiproliferative activity against Caco-2, HepG2, and K562 cell lines. The antiproliferative potential of (Ru/Ag/Pd)-Np was significantly improved following UV irradiation.

1. Introduction

Nanomedicine involves the use of the knowledge and tools of nanotechnology in the diagnosis, treatment, and prevention of disease and represents one of the most metamorphose ways in the future [1]. Nanometals have displayed a great interest in several innovative research fields. The activity, chemical, biological, physical, optical, and electrical properties of metal nanoparticles such as palladium (Pd), ruthenium (Ru), silver (Ag), platinum (Pt), and gold (Au) nanoparticles (NPs) depend on their particle shape and size [2].

Pd is a metal with fewer side effects and greater potential in biological applications than many other metals [3, 4]. Pd-NPs have been used as drug carriers, prodrug activators, and antibacterial, anticancer, antifungal, and antioxidant agents [5–8]. Pd-NPs showed promising therapeutic effects against cancer cells and multidrug-resistant bacteria and strong antibacterial/antibiofilm activities [9]. In addition, Pd (0) exhibited high efficacy as a therapeutic agent for human ovarian cancer [10]. Ag-NPs exhibited great success in several biological applications due to the large surface area of their particles [11]. Ag-NPs displayed antimicrobial, cytotoxic, and antiproliferative properties effects as previously reported [12–14]. Ru is a 4d transition metal widely used in

industrial and biological applications. Ru-NPs have a high surface area (1–3 m²/g) and hence could be used in catalysis and photocatalysis [15].

Some inorganic composites have emerged as attractive candidates in medicine due to their enormous surface area, conductivity, and high biological activity [16]. The green synthesis of Ag@Pd core-shell composite with enhanced anticancer activities using plant extracts was studied. When compared to WISH normal cells and the standard drug doxorubicin (DOX), the composite showed a significant antiproliferative activity against MCF7 and HEPG2 [17]. A nanoplate (Pd@Ag) core@silica shell composite was loaded with DOX and showed more potent antiproliferative activity by releasing DOX in response to heat and pH through the responsive coordination bonds [18]. A trimetallic Ti-Ag-Pd alloy with $\alpha + \beta$ -Ti structure has been synthesized and characterized. The Ti₉₄Ag₃Pd₃ alloy has great potential as a biomedical implant metallic composite [19]. Pd-Ag-decorated reduced graphene oxide (rGO) nanostructures were synthesized using a green chemical technique involving stevia extract and showed antibacterial potential under light irradiation. The biosynthesized Pd-Ag-decorated rGO nanostructures had good antibacterial action, inactivating 96% of *Escherichia coli* cells after 150 minutes of visible light irradiation. The study recommended that the nanostructured composite could be used for alternative nanomaterial-based medication development [20].

The citrate approach was used to make colloidal Ag@Pd core-shell nanoparticles (NPs) in aqueous media [21]. The antibacterial activity of Ag@Pd core-shell NPs was assessed qualitatively and quantitatively against model microbial species using the disc diffusion method to calculate the lowest inhibitory concentration. The inhibitory efficacy against bacteria and fungi was increased as the core-shell NPs concentration was raised to 25 mg/ml, demonstrating broad-spectrum actions.

Over the last few decades, the concept of green nanotechnology has grown, and sustainable methods of synthesis of nanoparticles were developed. The basic objectives of these methods include the synthesis of NPs using phytochemicals as simple, safe, ecofriendly, and cost-effective alternatives to toxic chemicals frequently used as reducing or capping agents [22]. Several bioresources have been used to create NPs of different sizes and forms, including plants, bacteria, fungi, yeasts, and algae [23]. Garlic (*Allium sativum* L.) possesses a wide antibiotic action against both Gram-positive and Gram-negative bacteria as well as antioxidant, anti-inflammatory, and anticancer activities. These beneficial effects were attributed to its rich content of bioactive molecules, including polysaccharides, organosulfur compounds, saponins, and phenolics [24].

This investigation aimed to synthesize and characterize a new trimetallic (Ru/Ag/Pd)-Np composite using *A. sativum* extract and to explore its antimicrobial and antiproliferative activities. In addition, the effect of UV irradiation on the antiproliferative activity of this nanocomposite was investigated.

2. Experimental

2.1. Instruments. Thermo Scientific Quattro S was used for scanning electron microscope (SEM) photodetection. An

IRTracer-100 SHIMADZU spectrophotometer was used for Fourier-transform infrared (FT-IR) measurements. X-ray diffraction (XRD) patterns were determined by XRD-7000 SHIMADZU via a copper radiation source. Thermal gravimetric analysis (TGA) was detected using TGA-51SHIMADZU with a heating rate of 10°C/min. A flow cytometer (BD FACSCalibur, USA) was used for cell cycle analysis. Japan's Shimadzu A LABOMED-Spectro 99 UV-Vis double beam-3200 was used to detect electronic spectra in the 200–800 nm range. A JEOL GEM-1010 transmission electron microscope operating at 80 kV was used to get the transmittance electron microscope (TEM) images.

2.2. Materials. The white tunicate leaf of *A. sativum* was collected from a local market in Sakaka, Saudi Arabia. The chemicals used in this study, namely, palladium acetate, ruthenium chloride, silver nitrate, 3-(4,5 dimethylthiazol-2-yl)-2,5-diphenyl tetrazolium bromide (MTT), and Annexin V-FITC apoptosis detection kit were supplied by Sigma-Aldrich (USA). All aqueous solutions were prepared using MilliQ water. Dulbecco's modified Eagle's medium (DMEM) and propidium iodide (PI) were purchased from Cambrex (New Jersey, USA) and Tianjin Dingsheng Xin (China), respectively. Human colon cancer (Caco-2), human hepatocellular carcinoma (HepG2), and human leukemia (K562) cells were supplied by VACSERA (Egypt). The antimicrobial activity of the prepared materials was tested against *Aspergillus flavus* (MT550030), *Aspergillus niger* (MW596373), *Candida albicans* (MW534712), *Candida glabrata* (MW865705), *Escherichia coli* (MW534699), and *Bacillus cereus* (MW830387). These isolates were obtained from the Biology Department, College of Science, Jouf University.

2.3. Green Synthesis of (Ru/Ag/Pd)-Np. The tunicate leaf of *A. sativum* (garlic) was collected and washed several times with tap and distilled water to remove debris and other contaminated contents and then dried at room temperature in the shade. Then, in 100 mL of distilled water, 3 g of the outer tunicate garlic leaves was boiled for 1 h to make the aqueous extract. The extract was filtered and mixed with 0.25 mmol of metal precursor (0.042 g of AgNO₃, 0.052 g of RuCl₃, and 0.056 g of Pd (CH₃COO)₂) in an aqueous solution. The color of the solution turned brown immediately, and the mixture was heated for 1 h at 50°C with stirring to allow the formation of a precipitate. To synthesize each nanometal, the extract was mixed separately with 0.042 g of AgNO₃, 0.052 g of RuCl₃, and 0.056 g of Pd (CH₃COO)₂, followed by the same steps. All precipitates were filtered through Whatman's No. 1 filter paper, then washed with hot distilled water, and dried in the air. The dried precipitates were preserved for all further characterization and biological studies.

2.4. Assessment of Cytotoxicity for (Ru/Ag/Pd)-Np before and after UV Exposure. Caco-2, HepG2, and K562 cells were cultured in DMEM supplemented with 10% fetal bovine

serum. The cells were trypsinized, seeded in 96-well plates, and treated with different concentrations of (Ru/Ag/Pd)-NP, nonirradiated or exposed to UV for 20 min, for 24 h. The MTT cell viability assay was used to determine the half-maximal inhibitory concentration (IC₅₀) in comparison to control cell growth. The optical density was measured at a wavelength of 570 nm [25].

2.5. Apoptosis Induction and Cell Cycle Analysis Assessment. Flow cytometry was used to assess cell cycle analysis and apoptosis [26]. Caco-2 cells were seeded and incubated in a CO₂ incubator at 37°C. The cells were then treated with (Ru/Ag/Pd)-NP before and after being exposed to UV light. The cells were collected, washed, fixed with cold alcohol, and incubated at 4°C for 2 h. After washing, the cells were stained with PI for 30 min at room temperature and protected from light. DNA content was determined by BD FACSCalibur, and cell cycle phase distribution was determined using Cell Quest Pro software (BD Biosciences, USA).

2.6. Annexin V-FITC Assay. Using fluorescently labeled Annexin V, the degree of apoptosis was also determined [26]. Briefly, Caco-2 cells were treated with the IC₅₀ of (Ru/Ag/Pd)-NP, before and after photoactivation, for 24 h. Then, the treated cells were harvested and washed in phosphate-buffered saline, and the degree of apoptosis was determined using a commercial kit.

2.7. Evaluation of Antimicrobial Activity of Metallic Np. The antimicrobial activity of the prepared NPs was tested against *A. flavus*, *A. niger*, *C. albicans*, *C. glabrata*, *E. coli*, and *B. cereus*. By using a 3 mm cork borer, 100 μ l of garlic leaf water extract and metallic nanoparticles Ag-NP, Ru-NP, Pd-NP, and (Ru/Ag/Pd)-NP composite were added to wells formed in the solid media (nutrient agar for bacteria and potato dextrose agar for fungi) which have been previously inoculated by spreading a freshly prepared inoculum over the entire agar). The fungal plates were incubated for 6 days at 26°C [27], whereas yeast and bacterial plates were cultured for 48 h at 30°C [28]. The percentage of inhibition rate was calculated using the following equation [29, 30]:

$$\text{Inhibition growth percentage} = \frac{MC - MT}{MC \times 100}, \quad (1)$$

where MC is the diameter of the inhibition zone around the control, MT is the diameter of the inhibition zone around the treated material, and minimum inhibitory concentrations (MICs) were determined. All the experiments were repeated three times.

3. Results and Discussion

In this study, a trimetallic (Ru/Ag/Pd)-NP composite was synthesized using an aqueous extract of *A. sativum* leaf, demonstrating how environmentally sustainable bio-resources may function as efficient reducing agents for the ecofriendly synthesis of NPs. The entire green synthesis,

characterization, and biological applications of bio-synthesized nanocomposite are shown in Scheme 1.

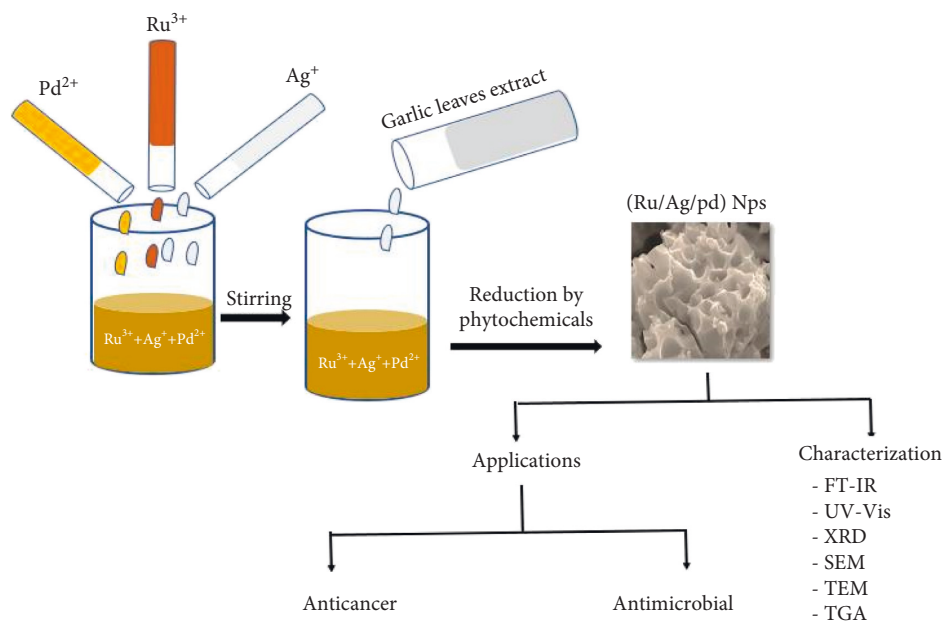
3.1. IR Spectra. The FT-IR spectra of solid garlic leaf and the synthesized composite in the spectral range of 500–4000 cm⁻¹ are depicted in Figure 1. The spectrum of solid garlic leaf revealed several bands at 3350, 2900, 1710, 1660, and 1160 cm⁻¹, which are attributed to stretching bonds of O-H, C-H, C=O, C=C, and C-O, respectively, found in bioorganic molecules such as phenolics, amino acids, and carboxylic acid compounds [31]. Allicin is the principal organosulfur compound in garlic [32]. Therefore, additional distinct bands associated with allicin were found at 800 cm⁻¹ (vC-S), 1050 cm⁻¹ (vS = O), and 1215 cm⁻¹ (vSS) [33]. On the other hand, the spectrum of the nanocomposite showed all of these vibrations with higher intensity due to weak van der Waals interactions between biochemical and metallic NPs [34]. New strong bands in the 550–600 cm⁻¹ range were observed, which are attributed to metal-metal interaction in the nanocomposite [35]. The new bands at 1610 and 1475 cm⁻¹ are often associated with the stretching and bending vibrations of the carboxylate anion (-COO), respectively, which is most likely caused by the oxidation of -C-OH in phytochemicals during the reduction of metal ions [36].

3.2. XRD. Figure 2 shows XRD patterns of the trimetallic nanocomposite. The positions of high-intensity peaks refer to the formation of pure (Ru/Ag/Pd) trimetallic NP. Peaks appeared at $2\theta = 40.11$, 47.75 , and 68.31 , which correspond to (111), (200), and (220), respectively, and are consistent with a conventional Pd-NP phase pattern (JCPDS: 87-0641) [37,38]. Ag-NP had typical peaks corresponding to the (111), (200), (220), and (311) planes at 2θ values of 38.45 , 44.85 , 67.55 , and 77.5 , respectively (JCPDS: 04-0783) [39]. For the hexagonal structure of Ru-NP, five different diffraction peaks were found and indexed with the planes (100), (002), (101), (102), and (110) at 38.42° , 43.82° , 46.12° , 58.32° , and 69.42° (JCPDS: 06-0663) [40]. No further impurity peaks were seen, indicating the presence of exclusively crystalline trimetallic NP. The size of the crystals was determined using the Scherrer equation [41, 42].

$$D = \frac{0.9 \cdot \lambda}{\beta \cdot \cos \theta}, \quad (2)$$

where $\lambda = 1.5418 \text{ \AA}$ is the wavelength of X-ray (for Cu K α 1), and θ is the XRD angle. β is the half-maximum width. The crystal size of the nanocomposite was calculated to be 15.67 nm.

3.3. TGA. TGA was used to assess the purity and thermal stability of composite NP (Figure 3). The weight of the nanocomposite decreased throughout the temperature range of 25–400°C, according to the TGA curve, showing that at higher temperatures, the organic compounds from the garlic leaf extract that served as the reducing agents in the formation of NP were completely decomposed (1.60% of the



SCHEME 1: Overall representation of synthesis, characterization, and bioapplications of (Ru/Ag/Pd)-Np.

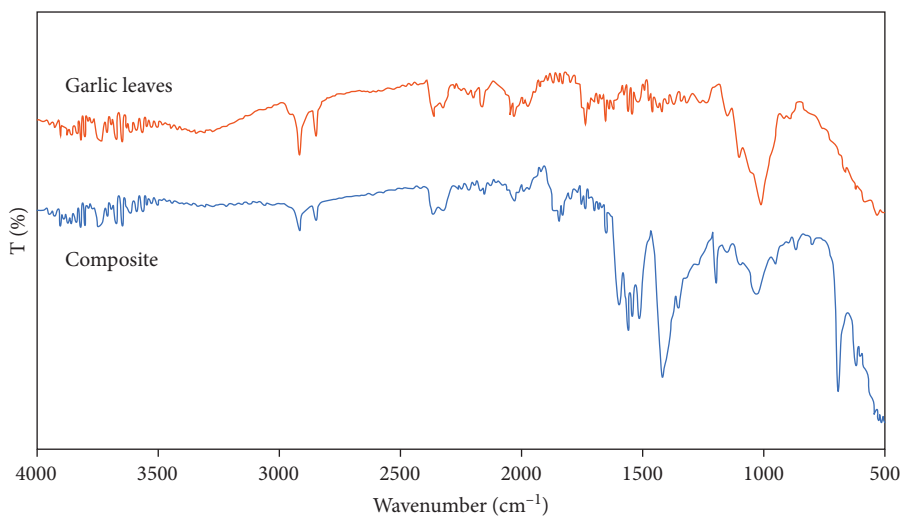


FIGURE 1: IR spectra of solid garlic leaf and (Ru/Ag/Pd)-Np.

original sample weight). Above 400°C, there was almost no deprivation, which accounts for the pure weight of the NP (98.40% of the original sample weight) [43].

3.4. Morphological Study. Using SEM imaging, the morphology of a nanocomposite was studied. SEM images were recorded and are shown in Figure 4. The trimetallic composite structure showed an irregular crystalline porous structure which is typical for metallic nanocomposites due to the strong interparticle contact imposed by the high surface energy. The bigger molecules of mixed nanostructures are formed when smaller nanostructures combine to form them. This may be seen in the SEM photos and is an indication of

nanocomposite formation [44]. TEM images show the spherical shape of nanoparticles with a particle size of 50–90 nm (Figure 5).

3.5. Absorption Spectra. The formation of metal NP is confirmed by absorption spectroscopy. Figure 6 shows the electronic spectra for both water *A. sativum* leaf extract and nanocomposite. Phytochemicals found in *A. sativum* leaf water extract are abundant and play a crucial function in the reduction methods used to produce metal NP [45]. A band at 280 nm in the absorption spectrum of the extract could be attributed to electronic transitions in the extracted phytochemicals [46]. The absorption spectrum of the

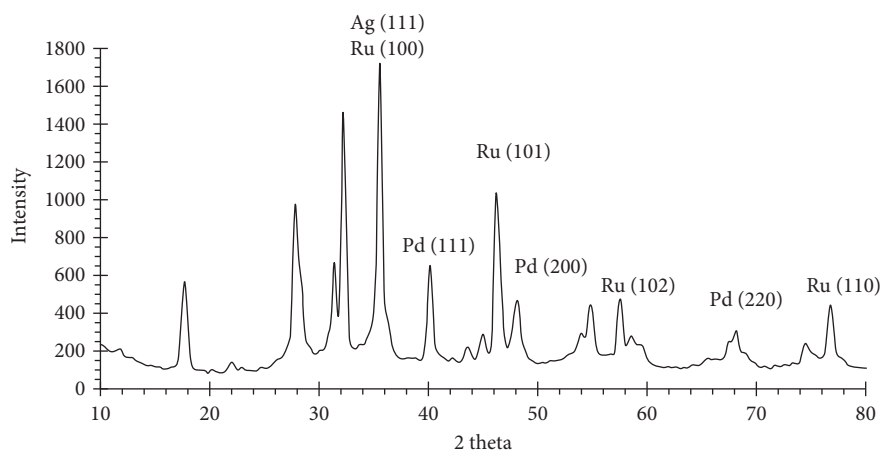


FIGURE 2: XRD of (Ru/Ag/Pd)-Np.

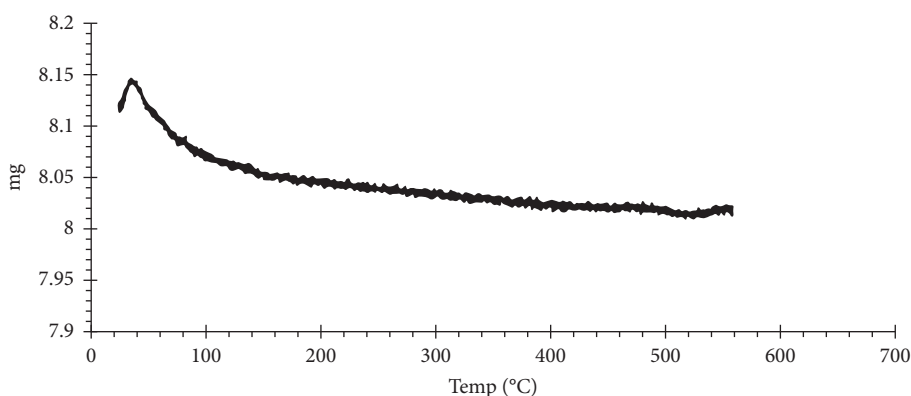


FIGURE 3: TGA of (Ru/Ag/Pd)-Np.

nanocomposite showed a distinct surface plasmon resonance, which is assigned by the appearance of the maximum absorption peak at 265 nm [47]. The absence of the bands assigned to Ag⁺, Pd²⁺, and Ru³⁺ in Figure S1 from the composite spectrum suggests that the nanocomposite formation follows precursor metal ion reduction.

3.6. In Vitro Anticancer Activity of (Ru/Ag/Pd)-Np before and after UV Exposure. The cytotoxic activity of (Ru/Ag/Pd)-NP before and after UV exposure was evaluated using Caco-2, HepG2, and K562 cells. Our data revealed that photoactivation markedly enhanced the anticancer efficacy of (Ru/Ag/Pd)-NP as represented in Table 1 and Figure 7.

Cell cycle arrest is a crucial mechanism through which anticancer drugs produce their antiproliferative effects [48, 49]. As a result, we investigated how (Ru/Ag/Pd)-NP, before and after UV exposure, affected the distribution of Caco-2 cells throughout the cell cycle. The purpose of the current study was to examine the cell cycle distribution and proliferation potential of Caco-2 cells following treatment with (Ru/Ag/Pd)-NP before and after UV exposure. To ascertain the total population distribution in the various phases (G0/G1, S, and G2/M), asynchronously growing Caco-2 cells were exposed to (Ru/Ag/Pd)-NP before and after UV

exposure for 24 h. The cells were then stained with PI and subjected to flow cytometry analysis.

Herein, Caco-2 cells were treated with the IC₅₀ of (Ru/Ag/Pd)-NP before photoactivation (47.35 μg/ml) and (Ru/Ag/Pd)-NP after photoactivation (9.32 μg/ml). (Ru/Ag/Pd)-NP before and after photoactivation induced apoptosis as indicated by an increase in the G2/M phase of 19.3% and 31.06%, respectively, in comparison with that of control Caco-2 cells (5.87%). Moreover, in the pre-G1 phase, (Ru/Ag/Pd)-NP before photoactivation resulted in apoptosis induction by 17.03%, while the photoactivated (Ru/Ag/Pd)-NP produced marked cells apoptosis by 32.41%, in comparison with that of control Caco-2 cells (2.23%) as represented in Figure 8. As a result, treatment with (Ru/Ag/Pd)-NP before and after UV exposure can encourage the transition of colon cancer cells from the G1 to the S phase and subsequently induce cycle arrest in the S phase, thereby weakening their ability to proliferate and decreasing their viability.

Apoptosis can be induced by arresting the cell cycle. The anticancer activities of NP synthesized by green synthesis have been proved in several investigations [50] showing that the cytotoxic activity was mediated by different mechanisms, including blocking cell cycle in G0/G1 [51] or G2/M [52] phases. In this study, we explored the impact of (Ru/Ag/Pd)-

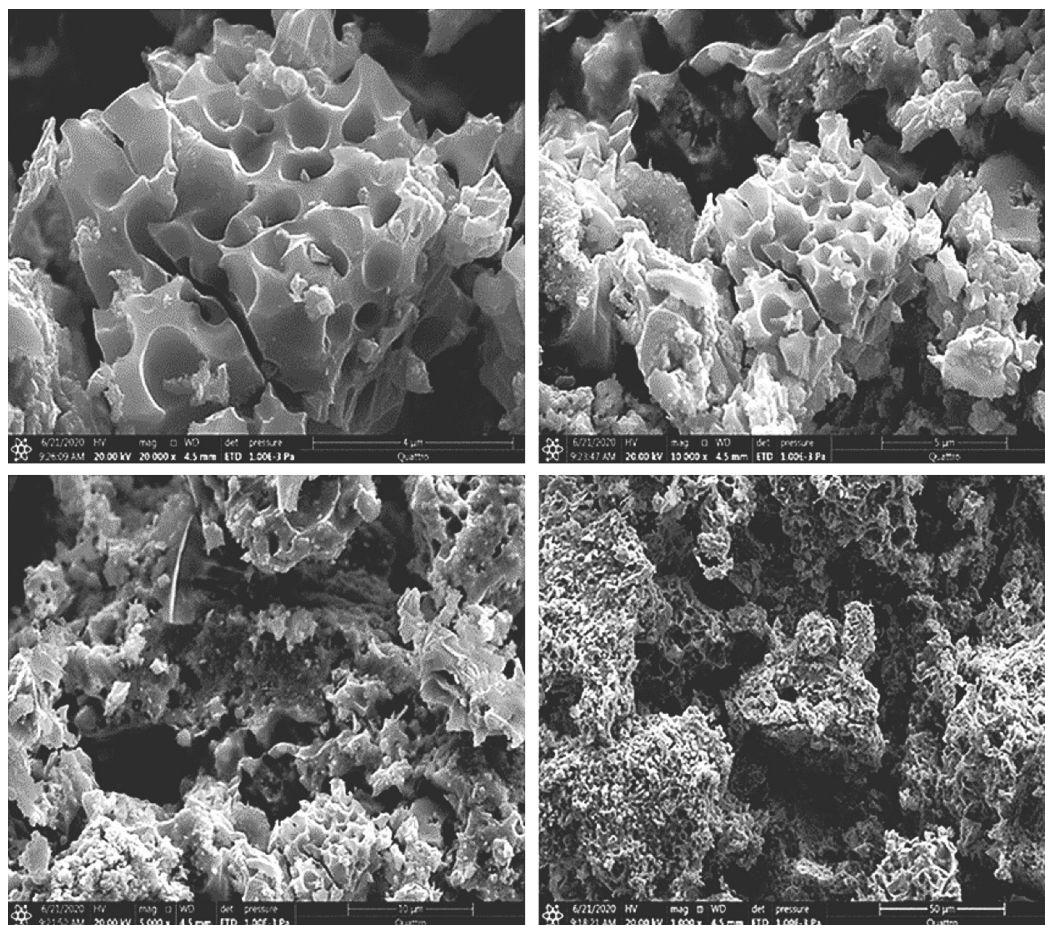


FIGURE 4: SEM images of (Ru/Ag/Pd)-Np.

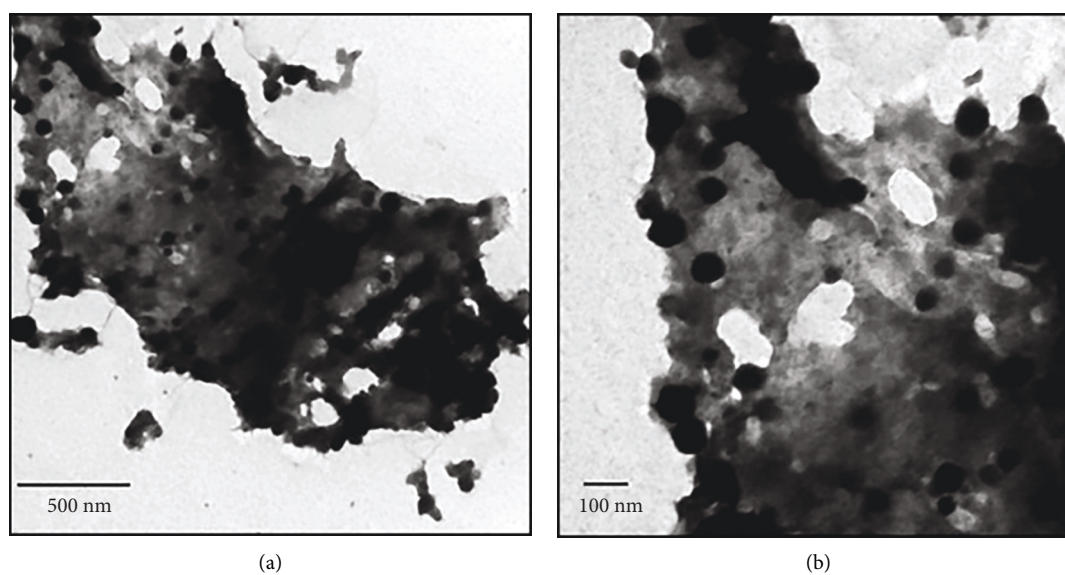
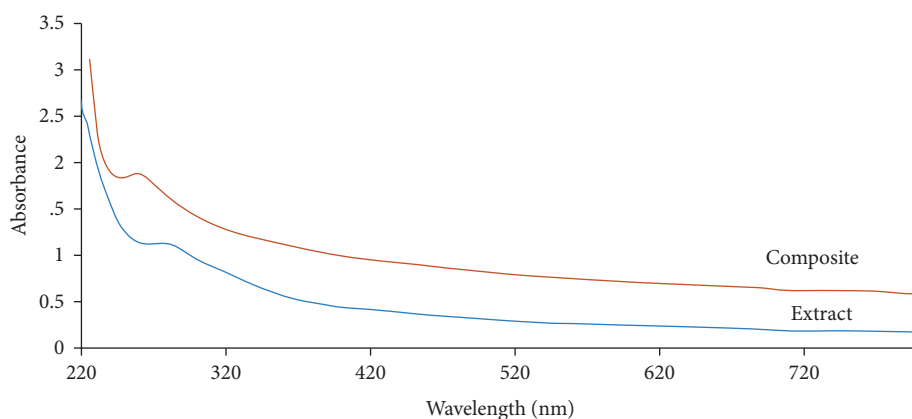


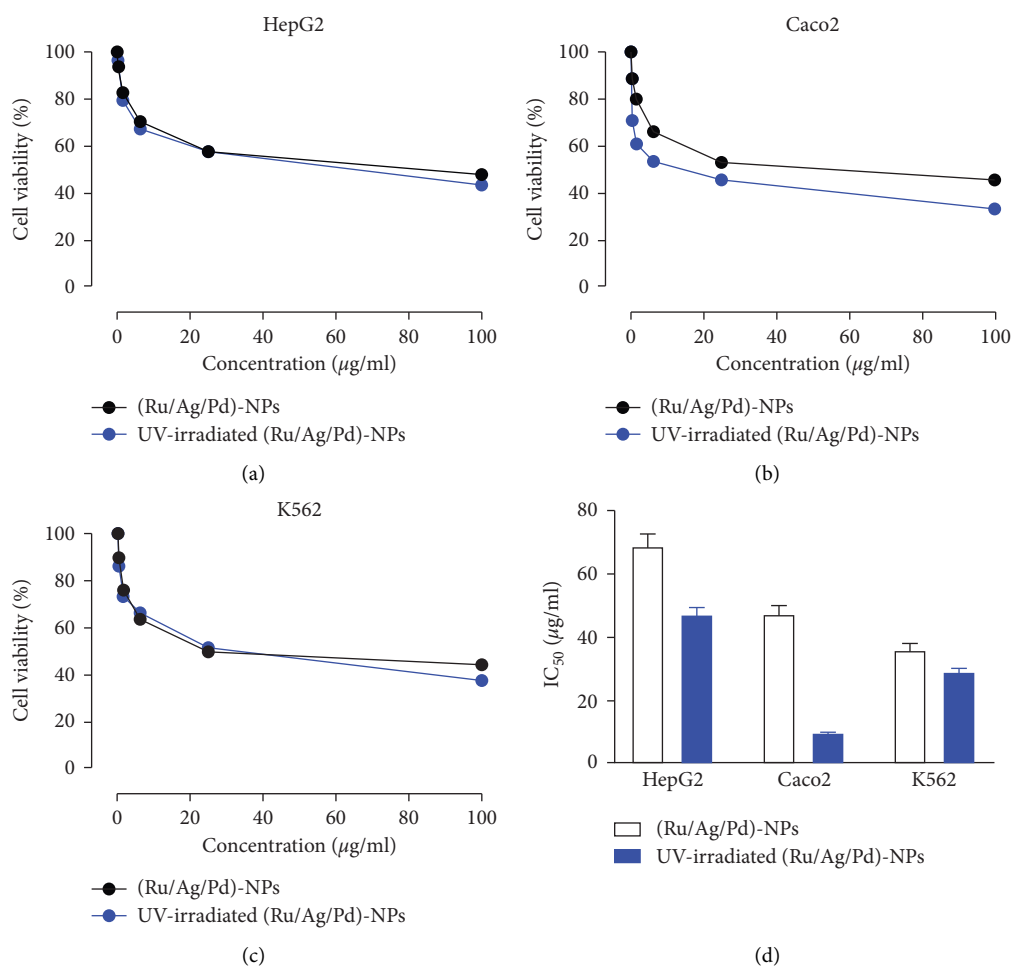
FIGURE 5: TEM images of (Ru/Ag/Pd)-Np.

NP on the ability of Caco-2 cells to undergo apoptosis before and after exposure to UV light. The presence of phosphatidylserine (PS) residues on the surface of the cell, which are typically concealed by the plasma membrane, is used for the

identification and quantification of apoptosis. One of the distinctive cues for macrophages to recognize and remove apoptotic cells is the presence of PS on the cell surface. Annexin V has demonstrated a high affinity for binding to

FIGURE 6: Electronic spectra of *A. sativum* extract and (Ru/Ag/Pd)-Np.TABLE 1: IC₅₀ values of (Ru/Ag/Pd)-Np against different cancer cell lines.

Tumor cell lines	IC ₅₀ before UV exposure ($\mu\text{g/ml}$)	IC ₅₀ after UV exposure ($\mu\text{g/ml}$)
Caco-2	47.35 ± 2.7	9.32 ± 0.52
HepG2	68.8 ± 3.9	46.77 ± 2.6
K562	35.87 ± 2.0	28.32 ± 1.6

FIGURE 7: UV exposure increases the cytotoxic activity of (Ru/Ag/Pd)-NP against (a) HepG2, (b) Caco-2, and (c) K562 cancer cell lines. (d) IC₅₀ values of the antiproliferative activity of (Ru/Ag/Pd)-NP on HepG2, Caco-2, and K562 cell lines. Data are mean \pm SD. The experiment was repeated three times ($N=3$).

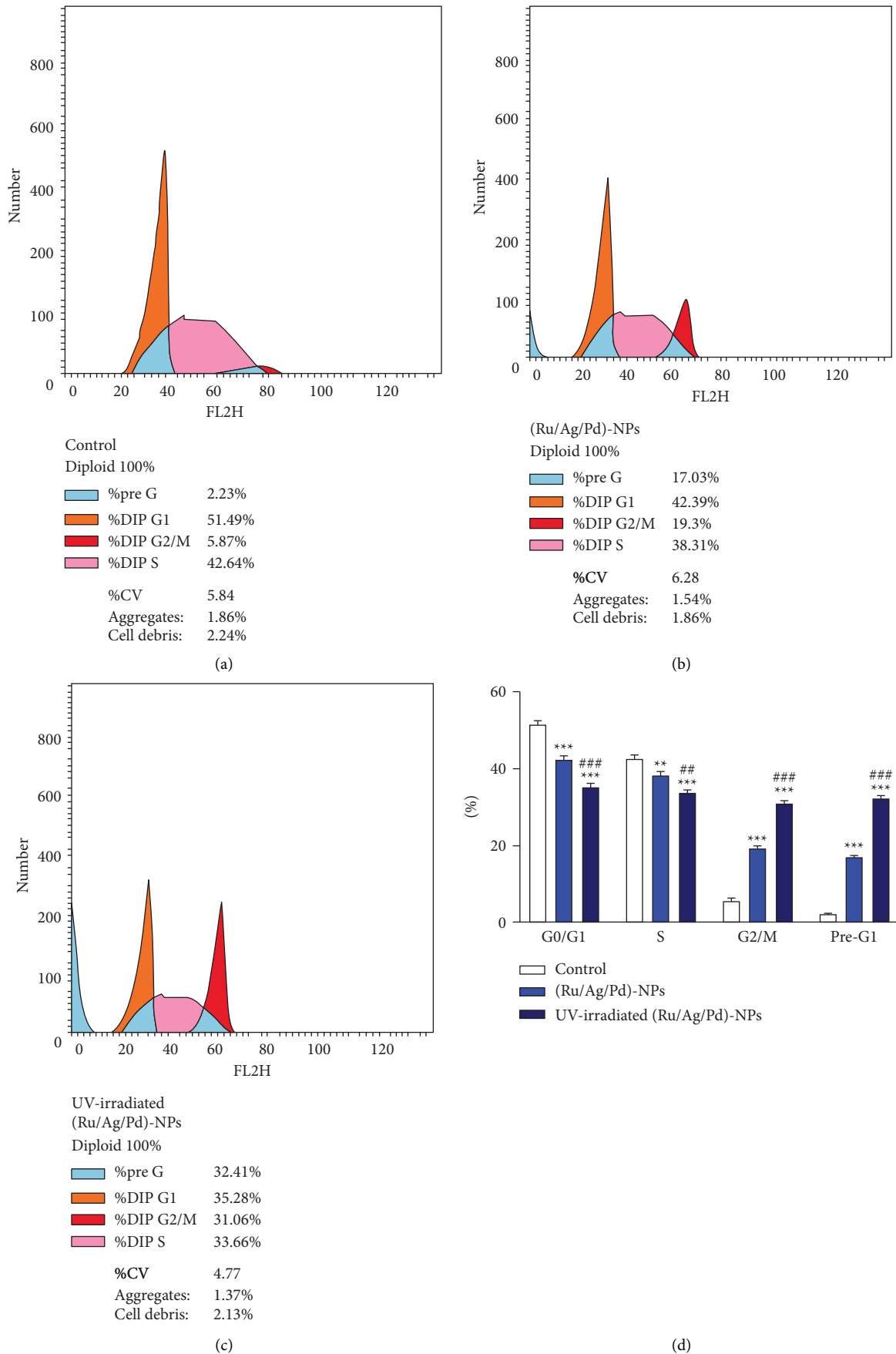


FIGURE 8: Representative histograms of DNA content distribution of cell cycle phases of control (a) and Caco-2 cancer cell line treated with (Ru/Ag/Pd)-NP before (b) and after UV exposure (c). (d) Percentage of the Caco-2 cells at different phases of the cell cycle. Data are mean \pm SD, $N = 3$. $**P < 0.01$ and $***P < 0.001$ versus control. $**P < 0.01$ and $***P < 0.001$ versus (Ru/Ag/Pd)-NP before UV exposure.

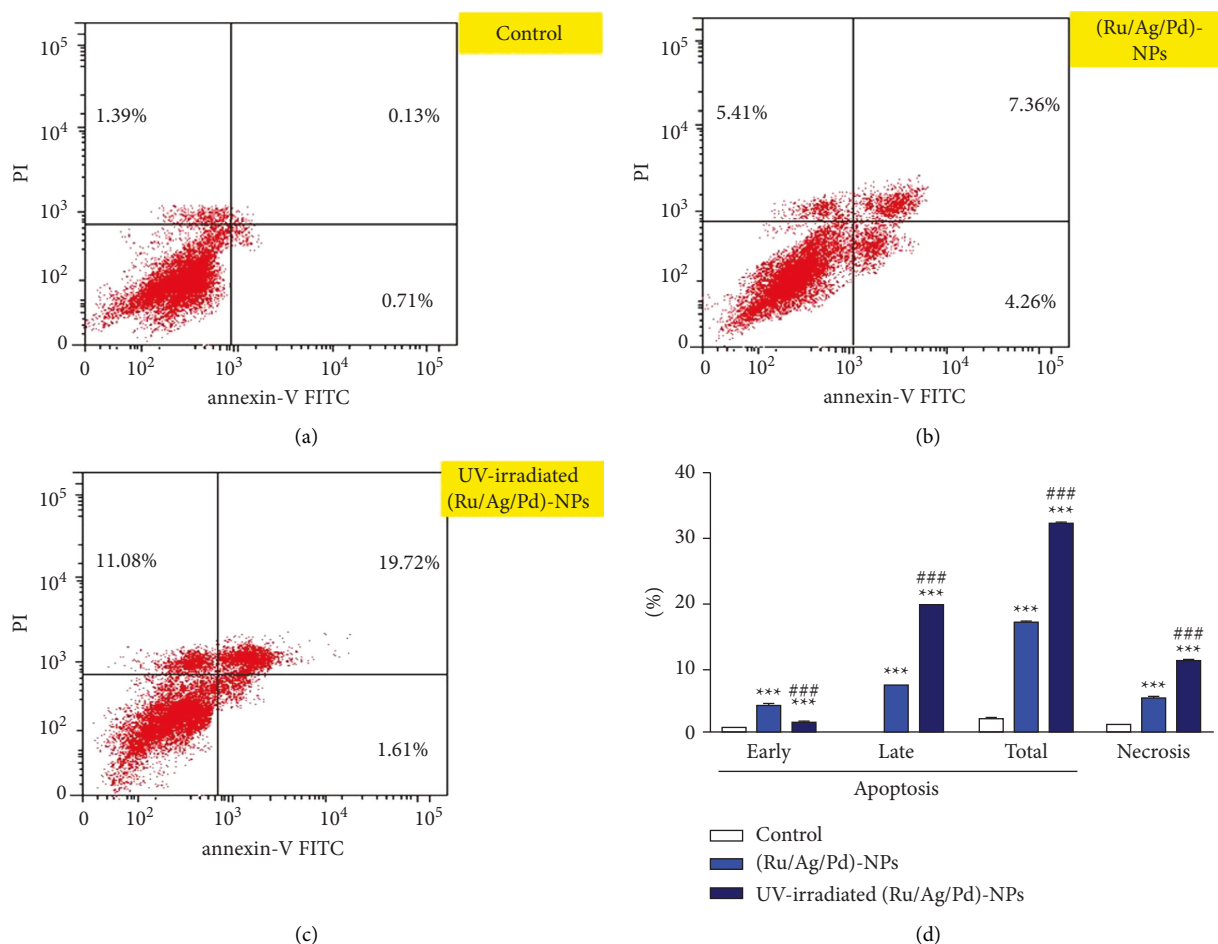


FIGURE 9: Representative blots of Annexin V/PI-stained control (a) and Caco-2 cancer cell line treated with (Ru/Ag/Pd)-NP before (b) and after UV exposure (c). (d) Percentage of Caco-2 cells exhibiting early and late apoptosis and necrosis following treatment with (Ru/Ag/Pd)-NP exposed to UV. Data are mean \pm SD, $N = 3$. *** $P < 0.001$ versus control and ### $P < 0.001$ versus (Ru/Ag/Pd)-NP before UV exposure.

PS and hence could be used to check the integrity of the cell membrane, which is compromised as the apoptotic process develops. It is feasible to discriminate between early and late apoptotic cells as well as dead cells using DNA-specific viability dyes such as PI [53].

Cell cycle analysis of the Caco-2 after treatment with (Ru/Ag/Pd)-NP either before or after photoactivation showed a preG1 peak that proved apoptosis (Figure 9). To confirm the effect of both (Ru/Ag/Pd)-NP on apoptosis induction and the impact of photoactivation, Caco-2 cells were stained with Annexin V/PI, incubated for 24 h, and analyzed. The results proved that both (Ru/Ag/Pd)-NP and its photoactivation potentially induced apoptosis in Caco-2 cells by 17.03% and 32.41%, respectively, in comparison with that of Caco-2 control cells (2.23%). These results indicated that photoactivation of the (Ru/Ag/Pd)-NP resulted in a 1.9-fold increase in its ability to induce apoptosis.

3.7. Antimicrobial Activity of (Ru/Ag/Pd)-NP. Six isolates of microbial strains, *A. flavus*, *A. niger*, *C. albicans*, *C. glabrata*, *E. coli*, and *B. cereus* were selected to evaluate the antimicrobial activity of the trimetallic NPs composite. MICs were

determined using four different dosages of nanomaterials (0.0125, 0.025, 0.05, and 0.1 mg/mL) (Figure 10). Table 2 shows the MIC experimental results. The nanocomposite's MIC value against the investigated microbes was 0.0125 mg/mL.

For comparison, antimicrobial experiments were carried out for every single metal as represented in Table 3 and Figure 11. The findings indicated that all tested materials demonstrated high antibacterial activity and followed the sequence

(Ru/Ag/Pd)-NP > Pd-NP = Ag-NP = Ru-NP > *A. sativum* extract in comparison to different isolate species of bacteria and fungus. Microbial growth inhibition was best with the composite (Ru/Ag/Pd)-NP.

To compare our findings with those of other studies, Table 4 displays the biological applications, synthesis techniques, and other characteristics of mono-, bi-, and trimetallic nanoparticles.

3.8. Mechanism of Bioactivity of NP. In this study, the high biological activity of (Ru/Ag/Pd)-NP could be attributed to its capacity to disrupt membranes, damage DNA, produce reactive oxygen species (ROS) such as peroxides and

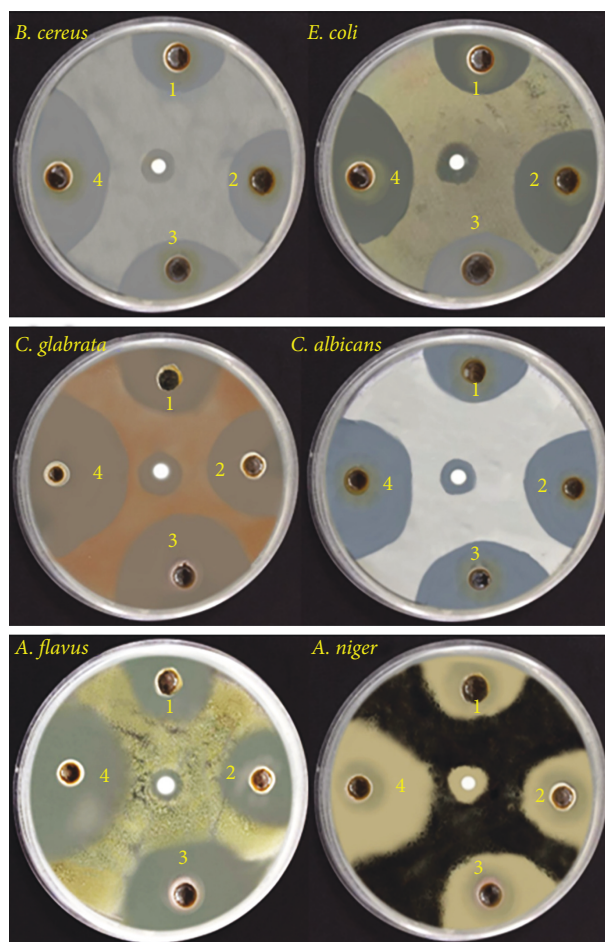


FIGURE 10: MICs results of (Ru/Ag/Pd)-NP (1) 0.0125 mg/mL, (2) 0.025 mg/mL, (3) 0.05 mg/mL, and (4) 0.1 mg/mL.

TABLE 2: MIC values in (mg/mL) of composite (Ru/Ag/Pd)-Np against different microbes.

Conc. of composite	Inhibition %					
	<i>A. flavus</i>	<i>A. niger</i>	<i>C. albicans</i>	<i>C. glabrata</i>	<i>E. coli</i>	<i>B. cereus</i>
(0.0125 mg/mL)	37.1	39.4	34.2	38.5	32.9	31.6
(0.025 mg/mL)	55.3	59.4	50	52.8	59.2	54.8
(0.05 mg/mL)	60.7	62.8	65.7	69.3	60.2	60.4
(0.1 mg/mL)	94.8	91.6	89.3	91.6	88.8	87.1

TABLE 3: Effect of different treatments of NPs at 0.0125 mg/mL concentration on growth %.

	% inhibition mycelia growth					
	<i>A. flavus</i>	<i>A. niger</i>	<i>C. albicans</i>	<i>C. glabrata</i>	<i>E. coli</i>	<i>B. cereus</i>
Control positive (miconazole)	—	—	32.7	—	—	—
Control positive (amikacin 30)	—	—	—	—	—	30.6
Garlic extract	19.7	15.5	20	14	20	19
Ag-NP	26.2	31.4	25	30	32.9	29.8
Pd-NP	24.9	29.7	32.4	29.5	25	27.4
Ru-NP	28.7	26.4	21.5	26.3	28.5	29.3
(Ru/Ag/Pd)-NP	37.1	39.4	34.2	38.5	32.9	31.6

superoxide, denaturant proteins, and inactivate enzymes. They can either stop bacterial growth or eliminate it. Similar to this, NP can saturate and adhere to fungal hyphae and

create insoluble compounds that damage the membrane, bind lipids and enzymes, and induce cell lysis by inactivating the sulfhydryl groups of the fungal cell wall [58, 59].

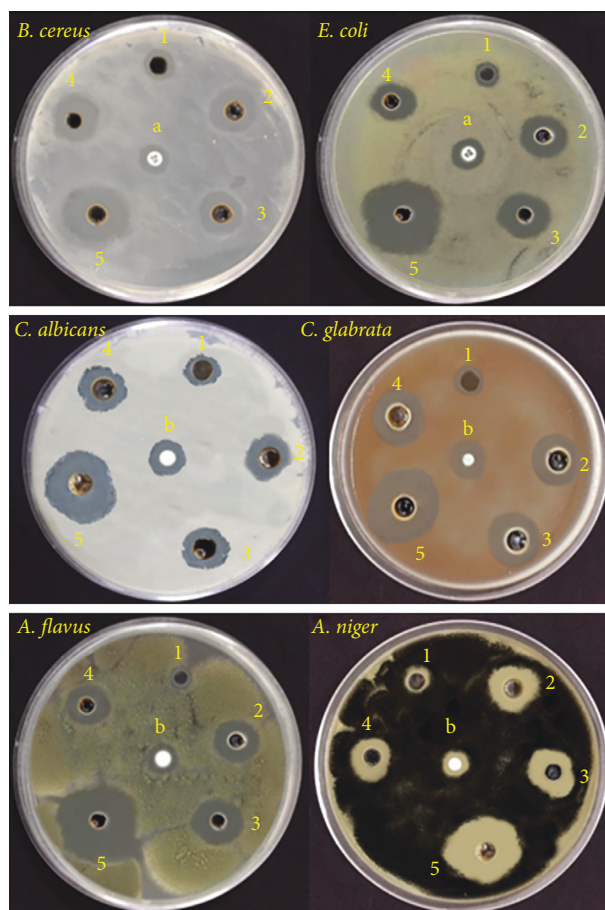


FIGURE 11: Effect of scale leaf of garlic (1), Ag-NP (2), Ru-NP (3), Pd-NPsp (4), and (Ru/Ag/Pd)-NP (5) on the growth of tested microbes, amikacin 30 (a) and miconazole (b).

TABLE 4: Comparison between biological activity using similar NPs.

NPs	Synthesis method	Particles size (nm)	Bio application	Average diameter inhibition zones (mm) against microorganisms tested	Reference
Ag	Green method via garlic leaf extract	20–70	Antimicrobial	11–24	[54]
Pd	Green method via brown alga, <i>Padina boryana</i>	11.16	Antimicrobial and anticancer	18–23	[9]
Ru	Green method via <i>Gloriosa superba</i> extract	25–90	Antibacterial	2.67–6.67	[55]
Ag/Pd	Chemical method via citrate reduction	9.8	Antimicrobial	1.4–1.9	[21]
Ag/Ru@GO	Chemical method via sodium borohydride	10–15	Antibacterial	0.5–9	[56]
Au/Pt/Ag	Microwave	20–40	Antimicrobial	14–17	[57]
(Ru/Ag/Pd)-NP	Green method via garlic leaf extract	15.67	Antimicrobial Anticancer	31.6–39.4 High anticancer activity	The current study

4. Conclusion

(Ru/Ag/Pd)-NP was synthesized using a green method. The nanocomposite was characterized with different physico-chemical techniques and its antiproliferative activity, before

and after UV exposure, was studied against HepG2, Caco-2, and K562 cancer cell lines. UV irradiation greatly improved the antiproliferative efficacy of the nanocomposite against all cancer cell types. In Caco-2 cells, (Ru/Ag/Pd)-NP caused cell cycle arrest, apoptosis, and necrosis, all of which were

enhanced by UV exposure. The antimicrobial activity of each single metal NP and the composite was determined against different bacterial and fungal strains. The highest activity appeared for the (Ru/Ag/Pd)-NP with a MIC value of 0.0125 mg/mL.

Data Availability

The data supporting the findings of this study are included within the article and its supplementary materials.

Disclosure

Some of the data included in the article were previously deposited as a preprint (<https://www.researchsquare.com/article/rs-1819275/v1.2>).

Conflicts of Interest

The authors declare that they have no conflicts of interest.

Acknowledgments

The authors would like to thank the Deanship of Scientific Research at Jouf University for funding this research (grant number DSR 2020-04-438).

Supplementary Materials

Additional data in this work are stated in the supplementary file. In the supplementary file, Figure S1 depicts the absorption spectra of metal precursors used in this work. (*Supplementary Materials*)

References

- [1] M. M. Rahman, F. Islam, S. Afsana Mim et al., "Multifunctional therapeutic approach of nanomedicines against inflammation in cancer and aging," *Journal of Nanomaterials*, vol. 2022, Article ID 4217529, 19 pages, 2022.
- [2] A. M. Abu-Dief, L. H. Abdel-Rahman, M. A. Abd-El Sayed, M. M. Zikry, and A. Nafady, "Green synthesis of AgNPs utilizing Delonix Regia extract as anticancer and antimicrobial agents," *ChemistrySelect*, vol. 5, no. 42, pp. 13263–13268, 2020.
- [3] A. M. Nassar, "Bioactive palladium azomethine chelates, a review of recent research," *Synthesis and Reactivity in Inorganic, Metal-Organic, and Nano-Metal Chemistry*, vol. 46, no. 9, pp. 1349–1366, 2016.
- [4] A. M. Nassar, A. M. Hassan, and S. S. Alabd, "Antitumor and antimicrobial activities of novel palladacycles with abnormal aliphatic CH activation of Schiff Base 2-[(3-phenylallylidene) amino] phenol," *Synthesis and Reactivity in Inorganic, Metal-Organic, and Nano-Metal Chemistry*, vol. 45, no. 2, pp. 256–270, 2015.
- [5] S. Azizi, M. Mahdavi Shahri, H. S. Rahman, R. Abdul Rahim, A. Rasedee, and R. Mohamad, "Green synthesis palladium nanoparticles mediated by white tea (*Camellia sinensis*) extract with antioxidant, antibacterial, and antiproliferative activities toward the human leukemia (MOLT-4) cell line," *International Journal of Nanomedicine*, vol. 12, pp. 8841–8853, 2017.
- [6] S. A. Fahmy, E. Preis, U. Bakowsky, and H. M. E.-S. Azzazy, "Palladium nanoparticles fabricated by green chemistry: promising chemotherapeutic, antioxidant and antimicrobial agents," *Materials*, vol. 13, no. 17, p. 3661, 2020.
- [7] Y. Liu, D.-D. Wang, L. Zhao et al., "Polypyrrole-coated flower-like Pd nanoparticles (Pd NPs@ PPy) with enhanced stability and heat conversion efficiency for cancer photothermal therapy," *RSC Advances*, vol. 6, no. 19, pp. 15854–15860, 2016.
- [8] I. Saldan, Y. Semenyuk, I. Marchuk, and O. Reshetnyak, "Chemical synthesis and application of palladium nanoparticles," *Journal of Materials Science*, vol. 50, no. 6, pp. 2337–2354, 2015.
- [9] H. Sonbol, F. Ameen, S. Alyahya, A. Almansob, and S. Alwakeel, "Padina boryana mediated green synthesis of crystalline palladium nanoparticles as potential nanodrug against multidrug resistant bacteria and cancer cells," *Scientific Reports*, vol. 11, no. 1, pp. 5444–5519, 2021.
- [10] S. Gurunathan, E. Kim, J. W. Han, J. H. Park, and J.-H. Kim, "Green chemistry approach for synthesis of effective anti-cancer palladium nanoparticles," *Molecules*, vol. 20, no. 12, pp. 22476–22498, 2015.
- [11] N. S. Al-Radadi and A. M. Abu-Dief, "Silver nanoparticles (AgNPs) as a metal nano-therapy: possible mechanisms of antiviral action against COVID-19," *Inorganic and Nano-Metal Chemistry*, pp. 1–19, 2022.
- [12] C. Greulich, J. Diendorf, T. Simon, G. Eggeler, M. Eppe, and M. Köller, "Uptake and intracellular distribution of silver nanoparticles in human mesenchymal stem cells," *Acta Biomaterialia*, vol. 7, no. 1, pp. 347–354, 2011.
- [13] C. Krishnaraj, E. Jagan, S. Rajasekar, P. Selvakumar, P. Kalaichelvan, and N. Mohan, "Synthesis of silver nanoparticles using *Acalypha indica* leaf extracts and its antibacterial activity against water borne pathogens," *Colloids and Surfaces B: Biointerfaces*, vol. 76, no. 1, pp. 50–56, 2010.
- [14] K. Venugopal, H. A. Rather, K. Rajagopal et al., "Synthesis of silver nanoparticles (Ag NPs) for anticancer activities (MCF 7 breast and A549 lung cell lines) of the crude extract of *Syzygium aromaticum*," *Journal of Photochemistry and Photobiology B: Biology*, vol. 167, pp. 282–289, 2017.
- [15] M. Y. S. Ali, V. Anuradha, R. Abishek, N. Yogananth, and H. Sheeba, "In vitro anticancer activity of green synthesis ruthenium nanoparticle from *Dictyota dichotoma* marine algae," *NanoWorld Journal*, vol. 03, no. 04, pp. 66–71, 2017.
- [16] M. Venu, S. Venkateswarlu, Y. V. M. Reddy et al., "Highly sensitive electrochemical sensor for anticancer drug by a zirconia nanoparticle-decorated reduced graphene oxide nanocomposite," *ACS Omega*, vol. 3, no. 11, pp. 14597–14605, 2018.
- [17] W. I. Abdel-Fattah, M. Eid, S. I. Abd El-Moez, E. Mohamed, and G. W. Ali, "Synthesis of biogenic Ag@ Pd Core-shell nanoparticles having anti-cancer/anti-microbial functions," *Life Sciences*, vol. 183, pp. 28–36, 2017.
- [18] W. Fang, J. Yang, J. Gong, and N. Zheng, "Photo- and pH-triggered release of anticancer drugs from mesoporous silica-coated Pd@ Ag nanoparticles," *Advanced Functional Materials*, vol. 22, no. 4, pp. 842–848, 2012.
- [19] V. Y. Zadorozhnyy, X. Shi, M. V. Gorshenkov et al., "Ti-Ag-Pd alloy with good mechanical properties and high potential for biological applications," *Scientific Reports*, vol. 6, no. 1, pp. 25142–25149, 2016.
- [20] K. Mallikarjuna, O. Nasif, S. Ali Alharbi et al., "Phytogenic synthesis of Pd-Ag/rGO nanostructures using stevia leaf

- extract for photocatalytic H₂ production and antibacterial studies,” *Biomolecules*, vol. 11, no. 2, p. 190, 2021.
- [21] E. A. Bakr, H. G. El-Attar, and M. A. Salem, “Colloidal Ag@Pd core-shell nanoparticles showing fast catalytic eradication of dyes from water and excellent antimicrobial behavior,” *Research on Chemical Intermediates*, vol. 45, no. 3, pp. 1509–1526, 2019.
- [22] L. H. Abdel-Rahman, B. S. Al-Farhan, D. Abou El-ezz, M. A. Abd-El Sayed, M. M. Zikry, and A. M. Abu-Dief, “Green biogenic synthesis of silver nanoparticles using aqueous extract of moringa oleifera: access to a powerful antimicrobial, anticancer, pesticidal and catalytic agents,” *Journal of Inorganic and Organometallic Polymers and Materials*, vol. 32, no. 4, pp. 1422–1435, 2022.
- [23] Z. Guan, S. Ying, P. C. Ofoegbu et al., “Green Synthesis of Nanoparticles: Current Developments and Limitations,” *Environmental Technology & Innovation*, vol. 26, Article ID 102336, 2022.
- [24] A. Shang, S.-Y. Cao, X.-Y. Xu et al., “Bioactive compounds and biological functions of garlic (*Allium sativum* L.),” *Foods*, vol. 8, no. 7, p. 246, 2019.
- [25] J. V. Meerloo, G. J. Kaspers, and J. Cloos, “Cell sensitivity assays: the MTT assay,” in *Cancer Cell Culture* Springer, Berlin Germany, 2011.
- [26] Z. Darzynkiewicz, X. Huang, and H. Zhao, “Analysis of cellular DNA content by flow cytometry,” *Current Protocols in Immunology*, vol. 119, no. 1, 2004.
- [27] S. M. N. Moustafa, R. H. Taha, H. M. A. Abdelzaher, and H. A. Elgebaly, “Novel biosynthesis of Ag-nanocomplex for controlling Verticillium wilt disease of olive tree,” *Archives of Phytopathology and Plant Protection*, vol. 55, no. 2, pp. 198–216, 2022.
- [28] C. Ramteke, T. Chakrabarti, B. K. Sarangi, and R.-A. Pandey, “Synthesis of silver nanoparticles from the aqueous extract of leaves of *Ocimum sanctum* for enhanced antibacterial activity,” *Journal of Chemistry*, vol. 2013, Article ID 278925, 7 pages, 2013.
- [29] S. M. Moustafa and R. H. Taha, “Mycogenic nano-complex for plant growth promotion and bio-control of *Pythium aphanidermatum*,” *Plants*, vol. 10, no. 9, p. 1858, 2021.
- [30] A. M. Elseman, A. E. Shalan, M. M. Rashad, A. M. Hassan, N. M. Ibrahim, and A. M. Nassar, “Easily attainable new approach to mass yield ferrocenyl Schiff base and different metal complexes of ferrocenyl Schiff base through convenient ultrasonication-solvothermal method,” *Journal of Physical Organic Chemistry*, vol. 30, no. 6, Article ID e3639, 2017.
- [31] T. Gabriel, A. Vestine, K. D. Kim, S. J. Kwon, I. Sivanesan, and S. C. Chun, “Antibacterial activity of nanoparticles of garlic (*Allium sativum*) extract against different bacteria such as *Streptococcus mutans* and *Porphomonas gingivalis*,” *Applied Sciences*, vol. 12, no. 7, p. 3491, 2022.
- [32] A. Magryś, A. Olender, and D. Tchorzewska, “Antibacterial properties of *Allium sativum* L. against the most emerging multidrug-resistant bacteria and its synergy with antibiotics,” *Archives of Microbiology*, vol. 203, no. 5, pp. 2257–2268, 2021.
- [33] L. S. Barreto, M. S. Tokumoto, I. C. Guedes, H. G. D. Melo, F. D. R. Amado, and V. R. Capelossi, “Evaluation of the anticorrosion performance of peel garlic extract as corrosion inhibitor for ASTM 1020 carbon steel in acidic solution,” *Matéria. Revista Internacional d’Art*, vol. 22, no. 3, 2017.
- [34] J. Z. Mbese and P. A. Ajibade, “Preparation and characterization of ZnS, CdS and HgS/poly (methyl methacrylate) nanocomposites,” *Polymers*, vol. 6, no. 9, pp. 2332–2344, 2014.
- [35] C. E. A. Botteon, L. B. Silva, G. V. Ccana-Ccapatinta et al., “Biosynthesis and characterization of gold nanoparticles using Brazilian red propolis and evaluation of its antimicrobial and anticancer activities,” *Scientific Reports*, vol. 11, no. 1, pp. 1974–2016, 2021.
- [36] A. M. Nassar, A. M. Elseman, I. H. Alsohaimi, N. F. Alotaibi, and A. Khan, “Diaqua oxalato strontium (II) complex as a precursor for facile fabrication of Ag-NPs@ SrCO₃, characterization, optical properties, morphological studies and adsorption efficiency,” *Journal of Coordination Chemistry*, vol. 72, no. 5–7, pp. 771–785, 2019.
- [37] A. A. Abdelwahab, A. Elseman, N. Alotaibi, and A. Nassar, “Simultaneous voltammetric determination of ascorbic acid, dopamine, acetaminophen and tryptophan based on hybrid trimetallic nanoparticles-capped electropretreated graphene,” *Microchemical Journal*, vol. 156, 2020.
- [38] A. M. Nassar and N. F. Alotaibi, “Eggshell recycling for fabrication of Pd@ CaO, characterization and high-performance solar photocatalytic activity,” *Environmental Science and Pollution Research*, vol. 28, no. 3, pp. 3515–3523, 2021.
- [39] S. Berhanu, F. Habtamu, Y. Tadesse, F. Gonfa, and T. Tadesse, “Fluorescence sensor based on polyaniline supported Ag-ZnO nanocomposite for malathion detection,” *Journal of Sensors*, vol. 2022, Article ID 9881935, 11 pages, 2022.
- [40] Z. Zhang, H. Liu, L. Ni, Z.-L. Zhao, and H. Li, “Scalable synthesis of hcp ruthenium-molybdenum nanoalloy as a robust bifunctional electrocatalyst for hydrogen evolution/oxidation,” *Journal of Energy Chemistry*, vol. 72, pp. 176–185, 2022.
- [41] E. Ibrahim, L. H. Abdel-Rahman, A. M. Abu-Dief, A. Elshafaie, S. K. Hamdan, and A. Ahmed, “Electric, thermoelectric and magnetic characterization of γ -Fe₂O₃ and Co₃O₄ nanoparticles synthesized by facile thermal decomposition of metal-Schiff base complexes,” *Materials Research Bulletin*, vol. 99, pp. 103–108, 2018.
- [42] A. Saadat, A. Banaei, P. Mcardle, and R. Jafari, “Spectral, structural, and antibacterial study of copper (II) complex with N₂O₂ donor schiff base ligand and its usage in preparation of CuO nanoparticles,” *Journal of Chemistry*, vol. 2022, Article ID 8913874, 13 pages, 2022.
- [43] S. Lohrasbi, M. a. J. Kouhbanani, N. Beheshtkhou, Y. Ghasemi, A. M. Amani, and S. Taghizadeh, “Green synthesis of iron nanoparticles using plantago major leaf extract and their application as a catalyst for the decolorization of azo dye,” *BioNanoScience*, vol. 9, no. 2, pp. 317–322, 2019.
- [44] Z. Chen, D. Rao, J. Zhang et al., “Highly active and CO-tolerant trimetallic NiPtPd hollow nanocrystals as electrocatalysts for methanol electro-oxidation reaction,” *ACS Applied Energy Materials*, vol. 2, no. 7, pp. 4763–4773, 2019.
- [45] A. A. El-Refai, G. A. Ghoniem, A. Y. El-Khateeb, and M. M. Hassaan, “Eco-friendly synthesis of metal nanoparticles using ginger and garlic extracts as biocompatible novel antioxidant and antimicrobial agents,” *Journal of Nanostructure in Chemistry*, vol. 8, no. 1, pp. 71–81, 2018.
- [46] M. Nasrollahzadeh, S. M. Sajadi, and M. Maham, “Green synthesis of palladium nanoparticles using Hippophae rhamnoides Linn leaf extract and their catalytic activity for the Suzuki-Miyaura coupling in water,” *Journal of Molecular Catalysis A: Chemical*, vol. 396, pp. 297–303, 2015.
- [47] Z. Vaseghi, O. Tavakoli, and A. Nematollahzadeh, “Rapid biosynthesis of novel Cu/Cr/Ni trimetallic oxide nanoparticles with antimicrobial activity,” *Journal of Environmental Chemical Engineering*, vol. 6, no. 2, pp. 1898–1911, 2018.

- [48] A. Eastman, "Cell cycle checkpoints and their impact on anticancer therapeutic strategies," *Journal of Cellular Biochemistry*, vol. 91, no. 2, pp. 223–231, 2004.
- [49] G. I. Shapiro and J. W. Harper, "Anticancer drug targets: cell cycle and checkpoint control," *Journal of Clinical Investigation*, vol. 104, no. 12, pp. 1645–1653, 1999.
- [50] A. Gour and N. K. Jain, "Advances in green synthesis of nanoparticles," *Artificial Cells, Nanomedicine, and Biotechnology*, vol. 47, no. 1, pp. 844–851, 2019.
- [51] M. Murali, S. Anandan, M. A. Ansari et al., "Genotoxic and cytotoxic properties of zinc oxide nanoparticles phyto-fabricated from the obscure morning glory plant *Ipomoea obscura* (L.) ker gawl," *Molecules*, vol. 26, no. 4, p. 891, 2021.
- [52] A. A. Alshatwi, J. Athinarayanan, and P. Vaiyapuri Subbarayan, "Green synthesis of platinum nanoparticles that induce cell death and G2/M-phase cell cycle arrest in human cervical cancer cells," *Journal of Materials Science: Materials in Medicine*, vol. 26, no. 1, pp. 7–9, 2015.
- [53] M. Van Engeland, L. J. Nieland, F. C. Ramaekers, B. Schutte, and C. P. Reutelingsperger, "Annexin V-affinity assay: a review on an apoptosis detection system based on phosphatidylserine exposure," *Cytometry*, vol. 31, no. 1, pp. 1–9, 1998.
- [54] M. Reda, A. Ashames, Z. Edis, S. Bloukh, R. Bhandare, and H. Abu Sara, "Green synthesis of potent antimicrobial silver nanoparticles using different plant extracts and their mixtures," *Processes*, vol. 7, no. 8, p. 510, 2019.
- [55] K. Gopinath, V. Karthika, S. Gowri, V. Senthilkumar, S. Kumaresan, and A. Arumugam, "Antibacterial activity of ruthenium nanoparticles synthesized using *Gloriosa superba* L. leaf extract," *Journal of Nanostructure in Chemistry*, vol. 4, no. 1, pp. 83–86, 2014.
- [56] P. Andal and Roopakala, "Graphene oxide supported ruthenium, silver and ruthenium-silver nanoparticles as catalyst with antibacterial activity," *Asian Journal of Chemistry*, vol. 30, no. 1, pp. 89–96, 2018.
- [57] N. Yadav, A. K. Jaiswal, K. K. Dey et al., "Trimetallic Au/Pt/Ag based nanofluid for enhanced antibacterial response," *Materials Chemistry and Physics*, vol. 218, pp. 10–17, 2018.
- [58] R. Algotiml, A. Gab-Alla, R. Seoudi, H. H. Abulreesh, M. Z. El-Readi, and K. Elbanna, "Anticancer and antimicrobial activity of biosynthesized Red Sea marine algal silver nanoparticles," *Scientific Reports*, vol. 12, no. 1, pp. 2421–2518, 2022.
- [59] G. B. Fields, "Mechanisms of action of novel drugs targeting angiogenesis-promoting matrix metalloproteinases," *Frontiers in Immunology*, vol. 10, p. 1278, 2019.